catalysts

MDPI

Article

Benzene Oxidation over Pt Loaded on Fly Ash Zeolite X

Yuri Kalvachev [1,*], Totka Todorova [1], Hristo Kolev [1], Daniel Merker [2] and Cyril Popov [2,*]

[1] Institute of Catalysis, Bulgarian Academy of Sciences, Acad. G. Bonchev St., bl. 11, 1113 Sofia, Bulgaria; t.todorova@ic.bas.bg (T.T.); hgkolev@ic.bas.bg (H.K.)
[2] Institute of Nanostructure Technologies and Analytics (INA), Center for Interdisciplinary Nanostructure Science and Technology (CINSaT), University of Kassel, Heinrich-Plett-Str. 40, 34132 Kassel, Germany; merker@cinsat.uni-kassel.de
* Correspondence: kalvachev@ic.bas.bg (Y.K.); popov@ina.uni-kassel.de (C.P.); Tel.: +359-29793989 (Y.K.); +49-5618044205 (C.P.)

Abstract: In the present study, zeolite X (FANaX) was synthesized from coal fly ash (FA) by a two-step high-temperature method. In order to follow the effect of different contaminants in the starting coal ash, zeolite X was also synthesized from pure chemicals according to a classical recipe (NaX). Iron was loaded on this reference zeolite with the amount which was contained in the coal FA. The final catalytic samples were obtained by wet impregnation of Pt nanoparticles on both types of zeolite crystals. The most active samples in the benzene oxidation were the platinum-modified ones and, among them, the Pt-impregnated FA zeolite (Pt FANaX). The comparison of the catalytic activity of Pt FANaX with the reference PtFe NaX zeolite showed a temperature difference of 10 °C in favor of Pt FANaX at 50% benzene conversion. From these results, it can be concluded that FA zeolites are a good, cheaper and environmentally friendly alternative to traditional zeolites, synthesized from pure chemicals, which can be applied in the preparation of catalysts for the purification of gaseous mixtures from harmful organic compounds.

Keywords: fly ash; zeolite X; Pt nanoparticles; catalytic oxidation; benzene

Citation: Kalvachev, Y.; Todorova, T.; Kolev, H.; Merker, D.; Popov, C. Benzene Oxidation over Pt Loaded on Fly Ash Zeolite X. *Catalysts* **2023**, *13*, 1128. https://doi.org/10.3390/catal13071128

Academic Editor: Benoît Louis

Received: 30 April 2023
Revised: 17 June 2023
Accepted: 18 July 2023
Published: 20 July 2023

1. Introduction

The increased energy consumption implies an increased release of coal fly ash (FA) from thermal power stations in the environment. About 800 million tons of FA per year are separated as a waste product from coal-fired power plants, and this amount is expected to grow. Only in India, more than 65,000 acres of the mainland are used to store coal ash [1,2]. Coal ash is characterized by low pH, high salinity, lack of beneficial substances for the soil and a number of toxic elements (heavy metals and radionuclides). Depending on the specific coal deposit, the toxic components vary, and different amounts of the following elements may be included: As, Be, B, Cd, Cr, Co, Pb, Hg, Se, Tl, V and others. The most common chemical composition of FA presents amorphous aluminosilicates (formed by Si and Al oxides) in combination with variable mineral structures, such as quartz, magnetite, hematite, anhydrite, lime, feldspar and small amounts of iron, sodium, potassium, calcium, titanium, etc. The disposal of FA is a real environmental risk, and its utilization a global challenge, as today only 15% of FA is used as additives in the production of cement, building materials, polymer fillers, light ceramic materials, materials with low dielectric constant, as well as for the preparation of geopolymers [3,4].

Due to the chemical, mineral and textural nature of the fly ash, it is a suitable initial material for the synthesis of zeolite structures. Thus, on one side, a certain amount of FA will be utilized, and on the other hand, a low-cost starting material will be used to obtain a product with a high added value. Zeolites are well known for their unique properties, which give them many advantages in the catalytic processes: large specific surface area, high diffusion of reagents in the volume, ion exchange properties, etc. [5,6]. By melting

the ash with an alkaline base, soluble aluminates and silicates are formed, which could be easily transformed into a zeolite phase [7–10]. The zeolites obtained by this method, in contrast to the natural and synthetic zeolites obtained from pure chemicals, contain a significant amount of iron oxides (γ-Fe_2O_3, α-Fe_2O_3, γ-Fe_3O_4) together with traces of other active metals, which is a precondition for their good catalytic activity [11,12]. Zeolite X belongs together with zeolite Y to the family of aluminosilicate molecular sieves with a faujasite-type structure (FAU). Zeolite X differs from zeolite Y by its Si/Al atomic ratio, which is typically in the range from 1 to 2 for the X-type and higher for the Y-type zeolite.

The catalytic activity of FA zeolites can be improved by post-synthesis wet impregnation of different active metal phases depending on the desired catalytic reaction. It is well known that the main part of industrially important catalysts for CO oxidation and combustion of volatile organic compounds (VOCs) belongs to the group of catalysts with applied noble metals [13–16]. The platinum catalysts demonstrate higher activity than the palladium ones in complete oxidation reactions of VOCs [17]. Chunyu Chen et al. [18] monitored the effect of the size and dispersion of platinum nanoparticles on the catalytic performance of Pt-ZSM-5 in the reaction of total toluene oxidation. By impregnation of platinum nanoparticles over H-BETA zeolite structure, Rubén López-Fonseca et al. [19] obtained catalytic systems suitable for the oxidation of chlorinated VOCs. They proved that the presence of humidity in the reaction system does not interfere with the catalyst's activity; on the contrary, it significantly helps to direct the process to HCl formation instead of the unwanted product Cl_2. According to the order of relative activity of catalysts in the CO oxidation proposed by Kummer [20], Pt and Pd-containing catalysts show the highest activity. The metal oxides of the transition elements are less active, but they are a good alternative to the noble metals due to their cost and availability. Iron oxides exhibit moderate activity in oxidative reactions, but they are attractive due to their high stability, low cost and the fact that they are not harmful to the environment. Investigations of iron catalysts for the purification of automotive gases from CO and propane were conducted by Walker et al. [21]. In the reaction of CO oxidation at 300 °C the authors established the following order of catalytic activity: $Fe_2O_3/Al_2O_3 > Fe_2O_3/TiO_2 \approx Fe_2O_3 > FeSbO_4 > FePO_4 > Fe_2(MoO_4)_3$. A characteristic of the iron catalysts is their ability to oxidize CO in oxygenated and deoxygenated media via the oxygen in their lattice. In addition, the obtained iron oxide is a catalyst in the disproportionation of CO to carbon and/or CO_2, which are less harmful [22,23]. Mojca Rangus et al. [24] found that mesoporous silica modified with iron oxides appeared as an efficient and low-cost catalyst for the elimination of VOCs. The authors showed that the highest activity was demonstrated by the mesoporous silicate with Fe/Si ratio = 0.01, which can be due to (1) the optimal concentration of Fe^{3+} species and (2) the facilitated diffusion of reagents in the disordered structure of mesoporous silica compared to mesoporous silicon materials with arranged porous structure.

In recent years, scientists have focused their efforts on the preparation of catalysts containing more than one type of metal nanoparticles [25–27]. In these systems, a synergetic effect is achieved, which helps to increase significantly the catalytic activity compared to that of the mono-metal catalysts. An example of such a catalytic system was presented by Li et al. [28], using silica as a support material on which Pt and Fe particles were loaded. In this work, the temperature of complete CO oxidation was reduced by 90 °C in comparison to the corresponding single catalysts. J. Li et al. [29] reported a highly efficient V-Cu/ZSM-5 catalyst used for the complete oxidation of toluene in flue gases. In the purification of flue gas systems, difficulties arise from the impurities of SO_2, which form sulfates on the catalytic surface inflicting poisoning of the catalysts. In their work [29], the authors reported that the introduction of V nanoparticles into the catalyst structure provided centers for the SO_2 attachment, protecting the Cu particles during the catalytic process. By a combination of more acid centers, due to facilitated electron transfer and improved reducibility at low temperatures, the conversion temperature of toluene was significantly reduced to 276 °C, which was 45 °C and 114 °C lower than that for the corresponding monometallic catalysts. A series of Ag bimetallic systems based on ZSM-5 was studied by

A. Jodaei [30] in the complete oxidation of ethyl acetate. In their work, the authors noted that the main factor influencing the efficiency of catalyst systems was the type of the second metal component (M_2 = Fe, Co and Mn) at an optimal ratio of Ag/M_2. Complete oxidation of the organic molecules occurred at a temperature of 250 °C by the Fe/Ag/ZSM-5 catalyst at established optimal amounts of Ag = 1.75 wt. % and Fe = 1.3 wt. %. From all examples mentioned above, it becomes obvious that the preliminary planning of the desired catalyst (type of support material, combination of metal nanoparticles, amount of deposited metal component, type of organic molecule, etc.) is essential for the formation of a highly active catalyst system with preset properties.

There are published works investigating the catalytic behavior of zeolite supports obtained from coal fly ash [31–35]. One example was given by K.S. Hui et al. [32] for the complete combustion of methane over zeolite 4A catalysts formed by hydrothermal synthesis from coal ash. The effects of synthesis duration, the presence of Fe in FA and the surface properties of the catalysts on the complete oxidation of a gas mixture of n-hexane, acetone, toluene and 1,2 dichlorobenzene were investigated [33,34]. It was reported that, over the time of crystallization, zeolite FA-X exhibited reduced activity as a result of blocking Fe-active centers. The loading of copper or cobalt increased the activity of FA catalysts up to 80% for the above gas mixture. In our study [35], the catalytic performance of zeolite X (synthesized from FA) and modified with 0.5 wt. % of Pt was investigated in the reaction of CO oxidation. Comparing the conversion over both platinum catalysts (synthesized from FA or pure chemicals), it was found that the temperature difference for 100% CO oxidation was only 20 °C in favor of the zeolite synthesized from pure chemicals. Despite the slightly lower conversion on the coal ash catalyst, we believe that it has the potential for future application as a catalyst for the oxidation of CO and volatile organic compounds.

Research on the use of fly ash zeolite X as a support of platinum catalysts in complete benzene oxidation has not been found in the reported literature.

The goal of this study is to develop an efficient catalyst based on coal fly ash modified with Pt for the complete oxidation of benzene. The production of such catalysts will utilize an environmentally harmful material from one side and will be very cost-effective from another. The used fly ash contains high amounts of silicon and aluminum, which makes it suitable for zeolite X synthesis. Nano-sized platinum nanoparticles were impregnated on the synthesized FA zeolite support in order to form highly active catalysts. Zeolite X was also synthesized from pure chemicals on which monometallic (Pt and Fe) and bimetallic (PtFe) nanoparticles were loaded. The obtained fly ash catalysts were tested in the complete oxidation of the highly stable benzene molecule.

2. Results and Discussion

Zeolites X was synthesized from fly ash (FANaX) and pure chemicals (NaX) following the procedure described in section Materials and Methods. The results from the analyses of the chemical composition of the fly ash and the synthesized zeolites are summarized in Table 1.

Table 1. Chemical composition of fly ash and synthesized zeolites X.

Samples, Composition in wt. %											
	SiO_2	**Al_2O_3**	**Na_2O**	**Fe_2O_3**	**CaO**	**K_2O**	**MgO**	**MnO**	**P_2O_5**	**TiO_2**	**Weight Loss on Calcination**
FA	54.50	23.95	0.76	10.21	2.14	3.43	2.62	0.07	0.15	1.09	0.8
NaX	39.90	25.84	15.62	-	-	-	-	-	-	-	18.23
FANaX	36.64	23.07	14.38	4.50	1.71	0.58	2.15	0.06	0.02	0.77	16.02

The powder diffraction patterns of zeolite X synthesized from chemicals (NaX) and its coal FA (FANaX) counterpart are presented in Figure 1A and B, respectively. The NaX phase can be identified by a group of reflections (d = 14.45; 8.85; 7.55; 5.74; 5.11; 4.82; 4.42;

3.82; 3.35; 2.95; 2.80) showing that a pure phase of zeolite X was synthesized from chemicals (Figure 1A) [36]. In addition, very low-intensity reflections at d = 6.26 and 3.61 are observed in the XRD pattern of the FANaX sample (Figure 1B), which indicates that besides zeolite X, a negligible amount of sodalite is formed using fly ash as a starting material.

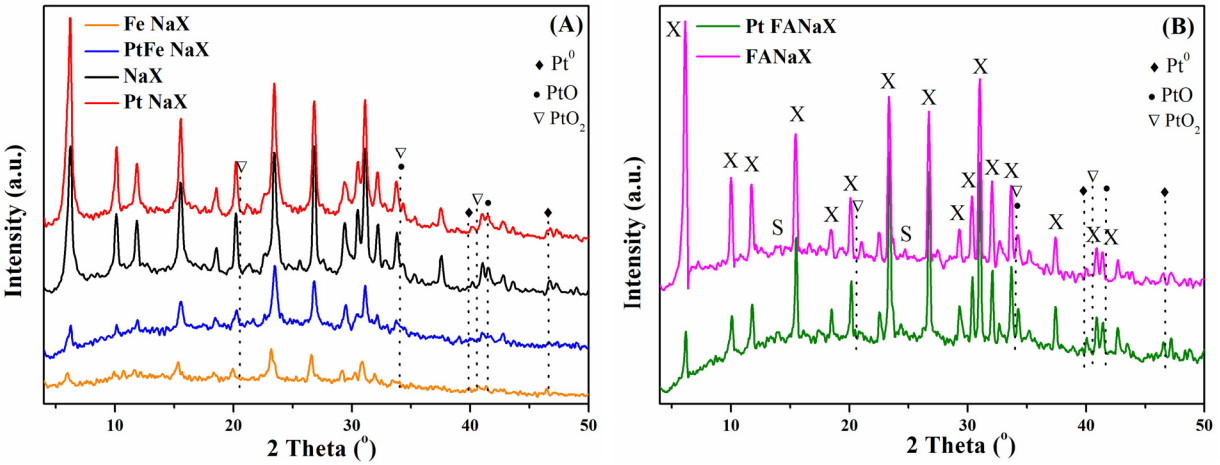

Figure 1. XRD patterns of (**A**) reference zeolite X obtained from chemicals (NaX) and its metal-impregnated analogs: Pt NaX, Fe NaX, PtFe NaX and (**B**) FA zeolite X (FANaX) and Pt impregnated FA sample with labeled diffraction peaks characteristic for zeolite X (X) and sodalite (S).

A main parameter for the quality of the fly ash zeolite is its degree of crystallinity. The yield of FANaX zeolite synthesized from the aluminosilicate part of the raw fly ash was evaluated on the order of 64% by comparison of the sum of relative intensities of selected peaks for the fly ash zeolite with the sum of relative intensities of the same peaks for the pure NaX zeolite, as described by S. Rayalu et al. [37], according to the formula:

$$X = \frac{\sum I_{Xi,exp}}{\sum I_{Xi,ref}} \frac{1}{(SiO_2 + Al_2O_3)} 100, \ [\%]$$

where X is the yield of the synthesized zeolite X from the alumosilicate mass of the raw fly ash, %; $\sum I_{Xi,exp}$ and $\sum I_{Xi,ref}$ are the sums of the intensities of X phase reflections in the experimental diffractograms of FANaX and NaX, respectively, arb. units; SiO_2 and Al_2O_3 are the contents of the corresponding components in the FA composition, mass%. Another approach to determine the degree of crystallinity of the fly ash zeolites is by using TGA [38].

High-activity catalysts were prepared by deposition of 0.5 weight percent Pt nanoparticles (Pt NaX and Pt FANaX samples—Figure 1A,B) onto both zeolite supports (from pure chemicals and FA). The preliminary results have shown that the loaded amount of Pt below 0.5% is insufficient, and the samples are not active. The diffraction peaks at 2θ = 39.9 and 46.6 correspond to the indexed planes (111) and (200), respectively, which are consistent with the fcc structure of Pt^0. The diffraction peaks at 2θ ~ 34.0 and 41.5 correspond to PtO. The diffraction peaks at 2θ ~ 20.5, 34.0, 40.5, and 40.4 are related to the indexed planes (001), (100), (101), and (002), respectively, consistent with the fcc structure of PtO_2. The absence of intense Pt-related diffraction lines can be attributed to the small amount of applied active phase in combination with its fine dispersion on the zeolite supports. In order to investigate the effect of iron impurities in the fly ash, the same amount of Fe contained in the fly ash zeolite was impregnated over the pure chemical zeolite X (Figure 1A, samples: Fe NaX and PtFe NaX). Analyzing these iron-containing samples with copper X-ray radiation yielded a high background level due to fluorescence. For this reason, the presence or absence of characteristic peaks corresponding to Fe_xO_y species [39,40] is questionable. However, from the presence of the background noise, we can speculate that Fe is present in both samples.

It can be seen that the peak intensity of (111) reflection significantly decreases after Pt loading on FANaX (Figure 1B), while it increases in the case of Pt NaX (Figure 1A).

This observation suggests that platinum occupies different positions in these two samples. Whereas on NaX, the platinum atoms are preferably situated on the external surface of the zeolite crystals, in the case of FANaX, the platinum atoms are trapped in the super cages and sodalite cages of the zeolite. This is also confirmed by the XPS results, shown below.

In Figure 2, SEM micrographs of zeolite X from chemicals (A), zeolite X from FA (B) and the initial coal fly ash (C) are presented. In images, A and B, the formation of a highly crystalline product with a typical octahedral morphology corresponding to zeolite X is observed. The reference zeolite X from pure chemicals (A) is composed of homogeneous crystallites with sizes of about 2–4 μm. In the FANaX sample (B), a complete transformation of the feedstock to well-formed zeolite crystals with dimensions close to those in the reference sample is observed.

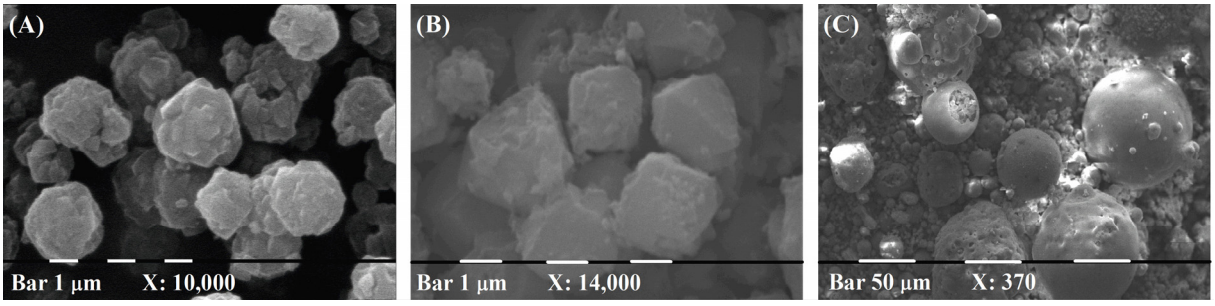

Figure 2. SEM images of (**A**) reference zeolite X obtained from chemicals (NaX), (**B**) zeolite X from fly ash (FANaX) and (**C**) starting fly ash.

The specific surface area and the micro-/mesopore volume of the reference and FA catalysts were investigated by physical adsorption of nitrogen (Table 2, Figure 3).

All studied catalysts form type I isotherms characteristic of microporous materials.

Comparing the textural characteristics of both zeolite supports (samples NaX and FANaX), it is obvious that zeolite X synthesized from pure chemicals owns better specific surface properties compared to the FA zeolite. Namely, the NaX sample has a larger active surface area and a larger pore volume (micro and total volume) than the support synthesized from FA. However, after the loading of iron on the NaX sample, the textural characteristics of the catalyst deteriorated significantly compared to those obtained from FA. There is lower N_2 uptake at lower pressure compared with other samples, followed by a gradual increase of N_2 uptake with the pressure increasing (Figure 3). The specific surface area, the microporous surface area and the pore volume are drastically reduced to 136 m^2/g (from 559 m^2/g in NaX), 18 m^2/g (from 496 m^2/g in NaX) and 0.24 cm^3/g (from 0.41 cm^3/g in NaX) for the Fe NaX sample (see Table 2). For comparison, the FANaX sample shows values of 386 m^2/g, 354 m^2/g and 0.27 cm^3/g for the respective parameters. The analysis of these results reveals that the additional impregnation of iron onto the zeolite structures leads to partial clogging of the crystal porous system and impairs the surface and diffusion properties of the material. The iron species in coal fly ash are positioned during the synthesis process in a way not to disrupt the molecular access to the crystal volume. Most likely, part of the Fe nanoparticles is involved in the construction of the zeolite crystal lattice, or they play the role of compensating ions. In the first case, during the synthesis, isomorphous replacement of T-atom with iron in the zeolite lattice occurred, and in the second case, iron is placed in ion-exchange positions.

When platinum is applied to FeNaX, the noble metal is preferably loaded on the external surface of the sample. A slight decrease in the total surface area of S_{BET} is observed. However, there is an increase in S_{mi}, most probably due to the textural inter-grain porosity. A comparison of the total pore volume of both samples—Fe NaX and FANaX with their Pt-loaded counterparts PtFe NaX and Pt FANaX, respectively, reveals a decrease of this parameter for both catalysts. It is less pronounced in the case of FANaX, where only a slight decrease of the micropore volume from 0.19 to 0.18 cm^3/g is observed. In the case

of PtFe NaX, the decrease of the total pore volume is larger, which is due to a reduction of the meso- and macropore volume without a change of the micropore volume. This fact shows once again that Pt is loaded preferably in the pore system of the sample FANaX and is finely dispersed, whereas on Fe NaX, it is loaded on the external surface of the sample, and the Pt dispersion is lower than on FANaX (see Table 2).

Table 2. Textural properties of investigated catalysts.

Sample	S_{BET} [a] [m^2/g]	S_{mi} [b] [m^2/g]	V_t [c] [cm^3/g]	V_{mi} [b] [cm^3/g]	V_{sec} [d] [cm^3/g]
NaX	559	496	0.41	0.27	0.14
Pt NaX	501	422	0.46	0.23	0.23
Fe NaX	136	18	0.24	0.01	0.23
PtFe NaX	127	23	0.19	0.01	0.18
FANaX	386	354	0.27	0.19	0.08
Pt FANaX	370	326	0.26	0.18	0.08

[a] BET surface area. [b] Microporous surface area and volume evaluated by V-t method. [c] Total pore volume. [d] Meso- and macropores volume ($V_{sec} = V_t - V_{mi}$).

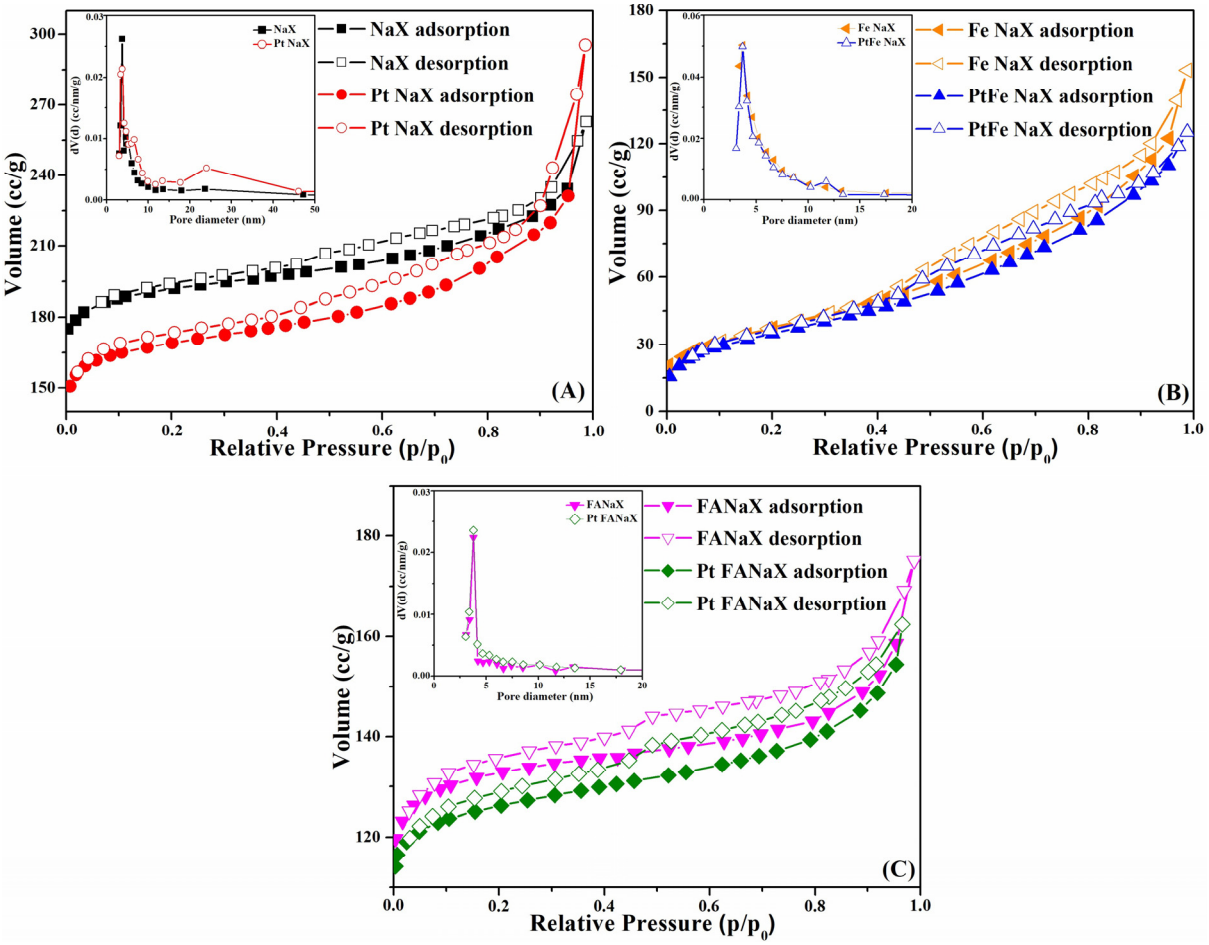

Figure 3. N_2 adsorption/desorption isotherms of the studied catalysts: (**A**) NaX and Pt NaX, (**B**) Fe NaX and PtFe NaX, (**C**) FANaX and Pt FANaX. Insets show the pore size distribution.

HRTEM images and particle size distribution are presented in Figure 4. The loaded Pt particles are with an average size of 2.1 nm in the case of the Pt FANaX sample and 3.9 nm in the case of the Pt FeNaX sample (more than 200 particles for each sample).

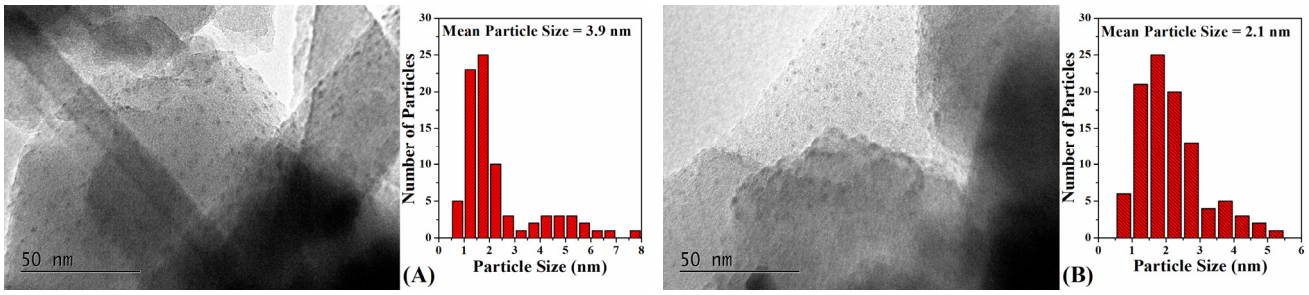

Figure 4. HRTEM imiges of Pt FeNaX sample (**A**) and Pt FANaX sample (**B**).

Like most silicates, the zeolites are based on TO_4 tetrahedra as primary building units, where T is an aluminum or silicon atom. The zeolite framework can be thought of as consisting of finite or infinite (i.e., chain- or layer-like) component units. The bonding of the primary building units between them leads to the formation of secondary building units and is a sign of the formation of a zeolite structure.

FTIR spectroscopy was also used to characterize the initial supports and the metal-impregnated catalysts—Figure 5. All investigated samples contain the IR characteristic bands at 1075, 981, 750, 665, 560 and 460 cm^{-1}, corresponding to the formation of a zeolite structure. The presence of a band at 981 cm^{-1} with a shoulder at 1075 cm^{-1} and a band at 560 cm^{-1} is assigned to the presence of the secondary building units, which form the structure of zeolite X. The spectra contain two additional bands at 3450 and 1640 cm^{-1} corresponding to the stretching mode of hydroxyl bonds and the scissors bending mode of the H_2O molecule, respectively.

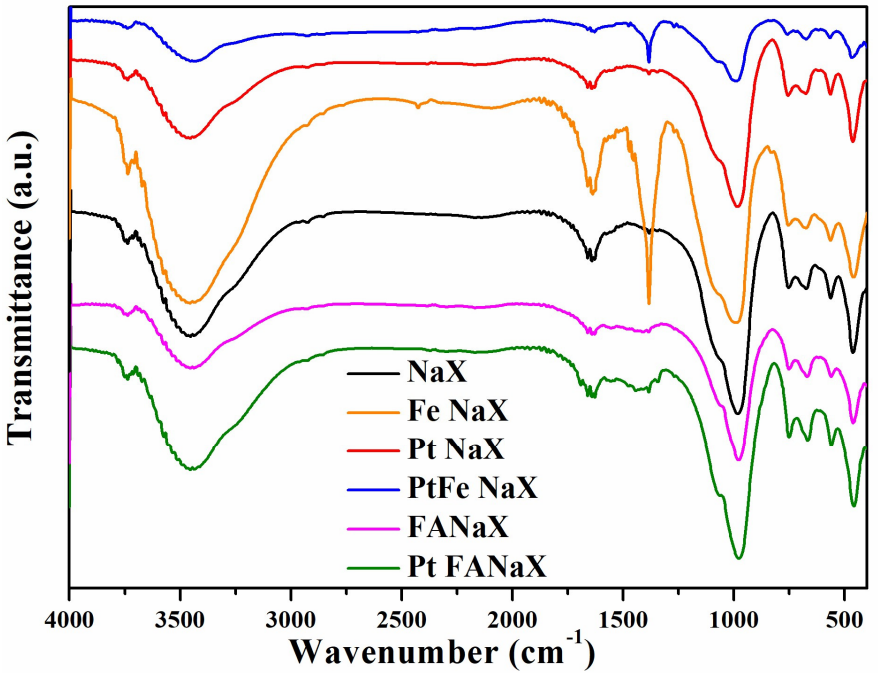

Figure 5. FTIR spectra of reference zeolite X (NaX), zeolite X from FA (FANaX) and their metal-impregnated samples: Fe NaX, Pt NaX, PtFe NaX and Pt FANaX.

The band at 981 cm^{-1} mentioned above can be attributed to the asymmetric stretching Si–O-T (T = Si or Al). Its position can be used to estimate the Si/Al ratio by a linear regression equation: $y = 0.0458x - 43.584$, where y is the Si/Al ratio, and x is the position of the band [41]. The calculated Si/Al ratio in the studied samples is 1.346, which is in good agreement with the results from the chemical analysis.

Table 3 contains the results of the XPS characterization used to determine the surface composition of the investigated samples. Traces of Mg, K and Ca are observed in the catalysts formed from fly ash, which is not the case for catalysts synthesized from pure chemicals. The FA samples demonstrate a slightly higher Fe surface content compared to the NaX catalysts. In the platinum-containing catalysts, a higher concentration of Pt nanoparticles on the surface of the catalysts from pure chemicals is detected compared to the FA catalysts. It corroborates the results from the XRD measurements assuming that some of the Pt particles are located in the zeolite channels or crystal defects of FA catalysts and hence their lower content on the crystal surface.

Table 3. The surface atomic concentration of studied samples derived from XPS data in at. %.

Sample	C1s %	O1s %	Al2p %	Si2p %	Na1s %	Mg1s %	Ca2p %	K2p %	Pt4f %	Fe2p %	N1s %
NaX	14.23	45.91	11.64	17.95	10.27	-	-	-	-	-	-
Fe NaX	6.30	53.78	11.58	19.51	6.59	-	-	-	-	1.50	6.59
Pt NaX	4.19	45.59	11.96	21.51	13.72	-	-	-	0.04	-	-
PtFe NaX	4.41	55.30	12.40	18.52	6.61	-	-	-	0.05	1.64	1.06
FANaX	5.18	50.47	7.88	19.16	11.17	2.05	1.19	0.44	-	2.46	-
Pt FANaX	4.95	48.74	8.83	18.53	10.75	2.38	2.84	0.41	0.02	2.56	-

Figure 6 shows the XP spectra of Fe2p and Pt4f core levels of the studied materials. Figure 4A represents the 4f level of platinum together with the 2p level of aluminum of both starting supports (NaX and FANaX) and their Pt-modified analogs. The overlapping of these two core levels brings some inaccuracy in the interpretation of the results. Nevertheless, using the curve fitting procedure, it is possible to extract information about the oxidation state of Pt. In the Pt sample synthesized from pure chemicals, the defined binding energy of Pt at about 72.5 eV can be subscribed to a Pt^{2+} oxidation state. Similar binding energy has been measured for PtO [42] and Pt_2Si [43] surfaces. Whereas the other two platinum samples, PtFe NaX and Pt FANaX, reveal an increase of the binding energy to about 73.0 eV, which can be prescribed to a strong interaction with the supports or even the formation of PtSi bondings [44]. Since there is no platinum peak at about 71 eV corresponding to metallic platinum, it can be concluded that the basic oxidation state of platinum in the samples prepared is 2+.

The Fe2p core levels were studied in the iron-containing catalysts (Figure 6B). To obtain the oxidation state of iron, we need to focus not only on the binding energy of the peak but also on the line shape or existence of satellites. In the Fe2p region, both pure chemical catalysts show two iron peaks with a binding energy of 711.8 eV and a satellite at 719.5 eV determining iron 3+ status. A satellite peak is also observed between peaks 3/2 and 1/2 for Fe^{3+}, but the signal is very weak, especially in the case of the FA catalysts. The shapes of the Fe peaks in the FA supports are very similar to those in the samples of the pure chemical, but a difference is observed in the binding energies. If the binding energy is more like that of Fe^{3+} in the FANaX sample, although $Fe^{2.5+}$ (like in Fe_3O_4—a mixture of Fe^{2+} and Fe^{3+} with a 1:1 ratio) cannot be ruled out with assurance [45,46], then in Pt FANaX sample Fe^{3+} dominates in the form of FeOOH or $NaFeO_2$ or a mixture of both phases [47,48]. The different binding energies in the PtFe FA catalyst are most likely due to modification with Pt. The obtained data give information about the oxidation state of iron atoms in the FA samples, but it cannot confirm with certainty whether some of them are in the zeolite structure or on the surface of the crystals in Fe^{3+} and/or $Fe^{2.5+}$ form.

The temperature-programmed reduction (TPR) method was used to monitor the reducibility of the prepared catalysts, which could be an indication of their catalytic activity in oxidation reactions. The TPR profiles of the two zeolite supports (pure chemicals NaX and coal fly ash FANaX) and their metal-impregnated analogs are presented in Figure 7. The pure chemical support does not show a pronounced reduction peak, which is characteristic of aluminum-silicate zeolite structures. However, the FANaX sample demonstrates two

overflow reduction peaks, one in the temperature range 350–500 °C and another in the range 530–700 °C. The difference in the reducing behavior of the two zeolite supports is attributed to the Fe content in the starting fly ash in combination with the impurities present in it, which is also proved by XPS analysis. From the table containing data for the surface compositions (Table 3), it is obvious that the amount of surface iron in the FA samples is higher than that in the samples obtained from pure chemicals. Despite the high content of Fe and the mentioned impurities in the FA sample, the reducing peaks exhibit a very low intensity. The reason is most likely that part of Fe is in non-reducible form, i.e., in the FA sample, most Fe atoms are in the state of metallic iron or participate in the structure of the zeolite framework.

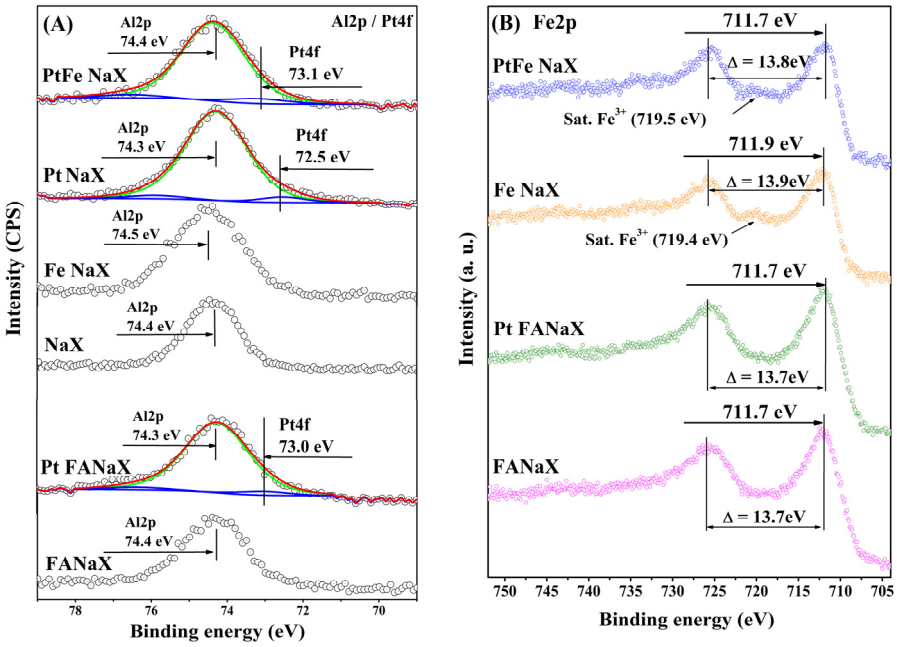

Figure 6. High-resolution XP Spectra of Al2p/Pt4f (**A**) and Fe2p (**B**) core levels in the studied NaX and FANaX samples. Blue line shows Pt4f doublet peak, whereas the green line - overlapping Al2p peak. The open circles represent the experimental data.

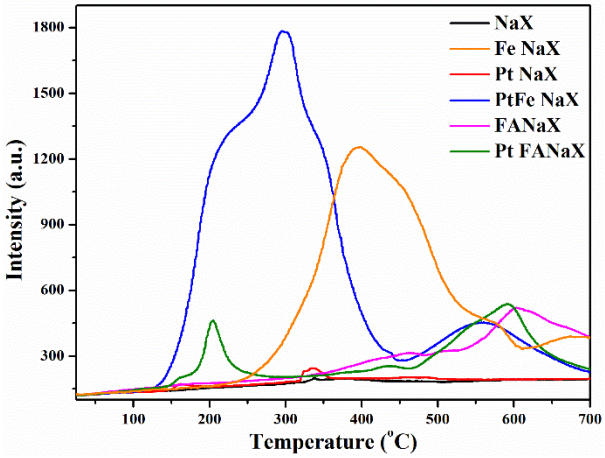

Figure 7. TPR profiles of reference zeolite X (NaX), zeolite X from FA (FANaX) and their metal-impregnated samples: Fe NaX, Pt NaX, PtFe NaX and Pt FANaX.

After the loading of iron on the pure chemical zeolite X, two clearly expressed signals occur: the first low-temperature reducing peak in a temperature range of 250–620 °C and a high-temperature peak above 620 °C. The presence of these two signals is due to the consecutive reduction of Fe_3O_4 and Fe_2O_3 species to metallic Fe. The temperature reduction

of iron is a relatively complex process that can take place through two or three stages. In both cases, in the first stage, an easy transition from Fe^{3+} (low-temperature signal) to Fe^{2+} takes place, and in the subsequent stages, a higher temperature is required for the transition of Fe^{2+} to Fe^{0}, directly and/or through a transition compound FeO. A. Pineau et al. [49] proposed in their work a mechanism of decomposition of Fe_3O_4 by the following equations:

(1) $3Fe_2O_3 + H_2 \rightarrow 2Fe_3O_4 + H_2O$
(2) $Fe_3O_4 + 4H_2 \rightarrow 3Fe + 4H_2O$
(3) $(1 - x)Fe_3O_4 + (1 - 4x)H_2 \rightarrow 3Fe(1 - x)O + (1 - 4x)H_2O$
(4) $Fe(1 - x)O + H_2 \rightarrow (1 - x)Fe + H_2O$

In our case, the low-temperature peak consists of two overlapping signals, i.e., during the reduction process in the FeNaX sample, the Fe species pass through the transition state FeO. If the presence of NO_3 ions (FTIR spectroscopy) in the Fe reference sample is taken into account, the decomposition of Fe $(NO_3)_3$-NaX to Fe_2O_3 and/or Fe_3O_4-NaX probably takes place in the first stage of heating.

The active catalysts (reference and FA samples) with loaded 0.5 wt. % Pt nanoparticles (Pt NaX, PtFe NaX and Pt FANaX samples) were also investigated by TPR. The TPR profile of the Pt sample synthesized from pure chemicals shows a very weak reduction peak in the range of 320–350 °C. The low intensity of the signal is most likely due to the oxidation state of platinum in combination with fine dispersion and the small amount of applied platinum salt. The PtFe NaX and Pt FANaX samples exhibited similar reduction behavior as Fe NaX, with the exception that the reduction peaks occurred at lower operating temperatures. In the PtFe NaX sample, a decrease of the reduction temperature by more than 100 °C is observed, while in the Pt FANaX sample, the decrease is about 200 °C compared to the Fe NaX sample. In other words, the Pt impregnation changes the reducing behavior of the catalysts to lower temperatures, and therefore it is expected to favorably affect the catalytic performance of these materials.

The activity of the studied catalysts was investigated in the complete oxidation of benzene, and the only formed products were H_2O and CO_2 (Figure 8). Tests with supposed intermediated products of partial oxidation, such as phenol, resorcinol, catechol, maleic anhydride, benzoquinone, and hydroxy-1,4-benzoquinone, were carried out. These compounds were injected as witnesses for detecting their retention time under identical GC conditions. In all cases, the benzene oxidation degree was complete—no intermediate products of partial oxidation were detected.

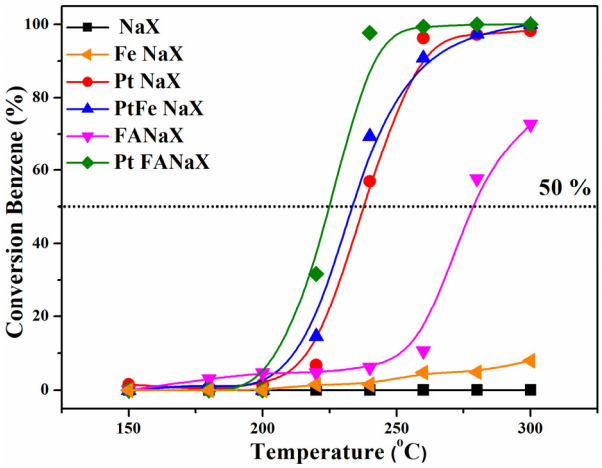

Figure 8. Temperature dependence of the conversion of benzene on reference zeolite X (NaX), zeolite X from FA (FANaX) and their metal-impregnated samples: Fe NaX, Pt NaX, PtFe NaX and Pt FANaX.

The following order of the catalytic activity was established from the temperature dependence of benzene conversion: NaX < Fe NaX < FANaX < Pt NaX < PtFe NaX < Pt FANaX. The catalysts are compared according to the temperature at which 50% conversion

of benzene was reached or according to the maximum achieved conversion in cases where this level of conversion is not implemented.

The active surface area and the pore volume of the PtFe NaX sample are much lower than the same parameters of Pt NaX (see Table 2), but the catalytic activity of both samples is close; even PtFe NaX has slightly higher catalytic activity. From this observation, it can be concluded that the presence of Fe species facilitated the benzene oxidation. The sample Pt FANaX shows better catalytic performance, and this can be due to the different nature of Fe species between Pt FANaX and PtFe NaX and from the presence of alkaline and alkaline earth metals, such as Mg, Ca and K.

The significantly higher activity of the FANaX support compared to the counterpart sample containing Fe is due to both better textual properties and the additional presence of Mg, Ca and K. The reduced catalytic behavior of Fe NaX can be attributed to the large amount of impregnated iron over the sample inflicting clogging of the porous structure, violating. As a result, the textural and diffusion properties of the catalyst. Evidence for this fact is the drastic decrease of the total surface area S_{BET} and especially the decrease of the surface area due to the presence of micropores in the zeolite structure S_{mi} (Figure 3, Table 2). As mentioned above, in the case of FANaX, the part of Fe is involved in the construction of the zeolite crystal lattice, or Fe plays the role of compensating ion, while in Fe, NaX iron is bulkier loaded on the zeolite surface. The different morphology of the samples Fe NaX and FANaX is due to the different ways of introducing iron in them. Fe is present In fly ash itself and, during the synthesis, is transferred to zeolite X, while in Fe NaX, iron is loaded additionally by impregnation. During the impregnation, the surface area decrease is observed, which is due to the blocking of pores.

The three platinum-containing samples (Pt NaX, PtFe NaX and Pt FANaX) were the most active and reached 100% conversion of benzene.

The higher catalytic activity of the Pt-modified fly ash sample is due to the simultaneous presence of redox pairs like Fe^{2+}/Fe^{3+}, Pt^{+}/Fe^{3+} and Pt^{+}/Pt^{0} species in the catalysts, which is very important for easier oxygen release. In the literature [32,33] Mars-van Krevelen mechanism is accepted for the VOCs oxidation, and most probably, the benzene oxidation follows this mechanism. According to the Mars-van Krevelen mechanism, the adsorption of VOC molecules on the catalyst's surface is the first step; their oxidation with lattice oxygen is followed by the oxidation of the reduced catalysts. The process of the adsorption of the organic molecules is an important step and can be affected by the surface properties of the catalysts. The presence of iron increases the mobility of the surface lattice oxygen and facilitates hydrocarbon oxidation. Hydrocarbon adsorption occurs at the Pt surface through π bonds and a back donation from the metal to the π^*-hydrocarbon orbitals. The vacant Pt^{2+} orbitals will be attracted to the π-electron-rich aromatic sites, and the electron transfer will result in organic molecule oxidation and Pt^{0} formation, transferring by the oxidizing system back to its initial Pt^{2+} state. Concerning benzene oxidation over zeolites supported Pd catalysts, Hea et al. have proposed initial $Pd^{2+}O^{2-}$ reduction by benzene followed by Pd^{0} oxidation with O_2 from the stream and $Pd^{2+}O^{2-}$ recovering [50]. Such redox process with gas phase oxygen supply prevails for nonreducible supports like alumina, whereas in our case, for reducible supports like FANaX, the lattice oxygen from iron oxides layers could participate in the redox transfer $Pt^{0} \leftrightarrow PtO$.

The most active sample is Pt FANaX. The difference in the temperature at which 50% conversion of benzene was reached between the Pt FANaX and the Pt-containing reference samples is 20 °C. The presence of stable redox pairs plays a key role in the Mars-van Krevelen mechanism, which is determined in the Pt FANaX sample by the presence of Fe, Mg, Ca, and Pt ions, making it more active. The loaded platinum is higher dispersed on the FANaX sample than on the Fe NaX one (see Figure 4). The Pt dispersion also is a factor for the higher catalytic activity of the Pt FANaX sample. An additional reason for the lower activity of the Fe NaX sample is the blocked pores, which makes the diffusion of reagents and products of the oxidation reaction through the zeolite pores more difficult.

The observed temperature for 100% complete benzene oxidation over Pt FANaX is higher than this of Pt/Al_2O_3 catalysts [51], and it is compatible with this of Au and Pd catalysts loaded on iron modified cerium oxides [52,53] and Mn/Co binary catalysts [54] and cobalt–cerium oxides [55]. The advantages are the utilization of fly ash from one side and a cheap source for the preparation of zeolite support from the other side.

3. Materials and Methods

3.1. Catalysts Preparation

Zeolite X (sample FANaX) was synthesized using coal fly ash as a starting reagent by double-stage heat treatment. During the first stage, the coal ash was melted with sodium hydroxide in a ratio of 1:2 at 550 °C temperature for 1 h. After the melting step, the coal ash was transferred into a polypropylene bottle, distilled water was added, and it was left for 24 h with constant stirring at room temperature. The second stage of the heat treatment involved the hydrothermal synthesis of the resulting solution for 22 h at 90 °C. The obtained zeolite material was washed with deionized water and dried for 20 h at 70 °C.

In order to trace the structural and chemical properties of zeolite X prepared from FA, a reference sample was synthesized from pure chemicals (NaX sample). The hydrothermal synthesis of the pure zeolite X was carried out from the initial gel composition $NaAlO_2$:$4SiO_2$:$16NaOH$:$325H_2O$ at 80 °C for 18 h. The used starting reagents were aqueous sodium silicate solution (Merck, Darmstadt, Germany), 99.99% pure aluminum powder (Acros, Geel, Belgium), 98+% sodium hydroxide (Chem-Lab, Zedelgem, Belgium) and distilled water.

Metal Pt and Fe nanoparticles were applied by wet impregnation using $Pt(NH_3)_4Cl_2xH_2O$ (Acros) and $Fe(NO_3)_3x9H_2O$ (Alfa Aesar, Kandel, Germany), respectively. Platinum nanoparticles with 0.5 wt. % (Pt FANaX sample) were applied to the zeolite support synthesized from fly ash, while 0.5 wt. % Pt and 4.5 wt. % Fe as a metal phase was applied onto the zeolite X from pure chemicals in order to investigate the effect of the impurities contained in the FA. After impregnation, the samples were calcinated at 350 °C.

3.2. Characterization

The catalysts synthesized from FA or pure chemicals were characterized by scanning electron microscopy (SEM), X-ray powder diffraction (XRD), TEM analysis, FTIR spectrometry, physical nitrogen adsorption/desorption method, temperature programmed reduction (TPR), and X-ray photoelectron spectroscopy (XPS). The powder diffraction patterns were collected on a D2 Phaser diffractometer Bruker, equipped with CuKa radiation at acceleration 30 kV and 10 mA current. The characterization conditions were 2θ = 4–50 scanned range at step value 0.04 min and time 2 s of acquisition. The high-resolution transmission electron microscopy (HRTEM) images were collected on HR STEM JEOL JEM 2100, equipped with a LaB6 electron source at an accelerating voltage of 200 kV. The specimens were prepared by grinding and dispersing the powders in ethanol by ultrasonic treatment for 6 min. The suspensions were dripped upon standard carbon/Cu grids. FTIR spectrometry data were collected on Bruker Tensor 37 spectrometer in the wavenumber region 4000–400 cm^{-1} at 64 scans for each sample, and resolution of 2 cm^{-1}. The physical nitrogen adsorption/desorption isotherms were measured with Quantachrome Instruments NOVA 1200e (Quantachrome Instruments, Boynton beach, FL, USA,) at a low temperature of 77 K. The t-plot and BJH methods were applied to determine the distribution of micro- and mesopores, while by BET equation, the specific surface area was calculated.

The X-ray photoelectron analyses (XPS) were performed on an ESCALAB MkII electronic spectrometer (VG Scientific, now Thermo Fisher Scientific, Waltham, MA, USA) possessing a twin anode MgKα/AlKα non-monochromated X-ray source using excitation energies of 1253.6 and 1486.6 eV, respectively. The measurements were performed only with an AlKα non-monochrome X-ray source at a chamber pressure of 9×10^{-9} mbar [56]. Gas chromatography (GC) equipped with the differential scanning calorimeter (DSC-111, SETARAM) was used to investigate the temperature-programmed reduction (TPR) prop-

erties of the catalysts. In order to remove the water from the gas stream, a cooling trap (−40 °C) was installed before the thermal conductivity detector. A mixture of hydrogen (10% H_2) and argon at a flow rate of 24 mL min^{-1} passed through a molecular sieve with size 5 A (−40 °C) before the sample reduction processes. During the experiments, the temperature was raised by a step of 15 °C min^{-1} from RT to 800 °C. The amount of sample used in the experiment was 0.05 g [57].

3.3. Catalytic Tests

The catalytic activity of the samples in the reaction of complete benzene oxidation, expressed as the degree of benzene conversion, was evaluated over the temperature range of 150–300 °C. A gas chromatograph (Hewlett Packard 5890 series II, Wilmington, DE, USA equipped with a flame ionization detector with a capillary HP Plot Q column was used to trace a gas mixture after contact with the catalysts. The catalytic oxidations were performed at samples of 0.5 cm^3 placed in a flow fixed bed micro-reactor at atmospheric pressure and temperature range of experiments 100–300 °C. The concentration of used benzene in all analyses was 42 gm^{-3} in air media at a space velocity of the gas flow 4000 h^{-1}. Before each experiment, the catalysts were activated at 350 °C for 1 h in an air environment.

4. Conclusions

In the present study, zeolite X was synthesized from coal FA by a two-step high-temperature method (melting step and hydrothermal step). In order to trace the effect of the iron contamination in the initial coal ash, the same amount of iron was applied by wet impregnation method on a reference sample prepared from pure chemicals. Platinum nanoparticles were deposited on both types of zeolite supports (reference and FA) to form catalysts suitable for the complete benzene oxidation reaction.

The most active samples in the benzene oxidation were the platinum-modified ones and, among them, the Pt-impregnated fly ash zeolite Pt FANaX. The comparison of the catalytic performance of Pt FANaX with that of the sample PtFe NaX showed that at 50% benzene conversion, the difference in the temperature was 10 °C in favor of the Pt FANaX sample. A large difference in the catalytic activity of benzene oxidation on FANaX and Fe NaX was observed, which can be due to the different states of iron in both samples. It was also observed that the presence of Fe and/or other metallic components as impurities in the coal ash favors the conversion process in the oxidation of benzene. From these results, it can be concluded that FA zeolites are a good, cheaper and environmentally friendly alternative to traditional zeolites, synthesized from pure chemicals, which can be applied in the preparation of catalysts for purification of gaseous mixtures from harmful organic compounds.

Author Contributions: Conceptualization, Y.K. and T.T.; methodology, T.T.; validation, Y.K., T.T. and H.K.; formal analysis, H.K. and T.T.; investigation, T.T., C.P. and D.M.; resources, D.M. and C.P.; writing—original draft preparation, Y.K., C.P. and T.T.; visualization, T.T.; supervision, Y.K. and C.P.; project administration, Y.K. and C.P. All authors have read and agreed to the published version of the manuscript.

Funding: This research was funded by the Bulgarian National Science Fund, grant number DN19/5 and by the Alexander von Humboldt Foundation.

Data Availability Statement: Data are contained within the article.

Acknowledgments: This work was supported by the Bulgarian National Science Fund (Contract No. DN 19/5). The authors would also like to acknowledge the financial support of the Alexander von Humboldt Foundation in the framework of the Research Group Linkage Program funded by the Federal Ministry of Education and Research (BMBF).

Conflicts of Interest: The authors declare no conflict of interest. The funder had no role in the design of the study; in the collection, analyses, or interpretation of data; in the writing of the manuscript, or in the decision to publish the results.

References

1. Babajide, O.; Musyoka, N.; Petrik, L.; Ameer, F. Novel zeolite Na-X synthesized from fly ash as a heterogeneous catalyst in biodiesel production. *Catal. Today* **2012**, *190*, 54–60. [CrossRef]
2. Ojha, K.; Pradhan, N.C.; Samanta, A.N. Zeolite from fly ash: Synthesis and characterization. *Bull. Mater. Sci.* **2004**, *27*, 555–564. [CrossRef]
3. Vilakazi, A.Q.; Ndlovu, S.; Chipise, L.; Shemi, A. The Recycling of Coal Fly Ash: A Review on Sustainable Developments and Economic Considerations. *Sustainability* **2022**, *14*, 1958. [CrossRef]
4. Ozturk, M.; Karaaslan, M.; Akgol, O.; Sevim, U.K. Mechanical and electromagnetic performance of cement based composites containing different replacement levels of ground granulated blast furnace slag, fly ash, silica fume and rice husk ash. *Cem. Concr. Res.* **2020**, *136*, 106177–106185. [CrossRef]
5. Kalvachev, Y.; Todorova, T.; Popov, C. Recent progress in synthesis and application of nanosized and hierarchical Mordenite—A short review. *Catalysts* **2021**, *11*, 308. [CrossRef]
6. Auerbach, S.M.; Carrado, K.A.; Dutta, P.K. *Handbook of Zeolite Science and Technology*, 1st ed.; CRC Press: London, UK, 2003; pp. 1–1204.
7. Querol, X.; Moreno, N.; Umana, J.C.; Alastuey, A.; Hernandez, E.; Lopez-Soler, A.; Plana, F. Synthesis of zeolites from coal fly ash: An overview. *Int. J. Coal Geol.* **2002**, *50*, 413–423. [CrossRef]
8. Murayama, N.; Yamamoto, H.; Shibata, J. Zeolite synthesis from coal fly ash by hydrothermal reaction using various alkali sources. *J. Chem. Technol. Biotechnol.* **2002**, *77*, 280–286. [CrossRef]
9. Derkowski, A.; Franus, W.; Beran, E.; Czímerová, A. Properties and potential applications of zeolitic materials produced from fly ash using simple method of synthesis. *Powder Technol.* **2006**, *166*, 47–54. [CrossRef]
10. Kalvachev, Y.; Zgureva, D.; Boycheva, S.; Barbov, B.; Petrova, N. Synthesis of carbon dioxide adsorbents by zeolitization of fly ash. *J. Therm. Anal. Calorim.* **2016**, *124*, 101–106. [CrossRef]
11. Boycheva, S.; Zgureva, D.; Miteva, S.; Marinov, I.; Behunová, D.M.; Trendafilova, I.; Popova, M.; Václaviková, M. Studies on the Potential of Nonmodified and Metal Oxide-Modified Coal Fly Ash Zeolites For Adsorption of Heavy Metals and Catalytic Degradation of Organics for Waste Water Recovery. *Processes* **2020**, *8*, 778. [CrossRef]
12. Shokanov, A.; Vereshchak, M.; Manakova, I. Mössbauer and X-ray Studies of Phase Composition of Fly Ashes Formed after Combustion of Ekibastuz Coal (Kazakhstan). *Metals* **2020**, *10*, 929. [CrossRef]
13. Spivey, J.J. Complete catalytic oxidation of volatile organics. *Ind. Eng. Chem. Res.* **1987**, *26*, 2165–2180. [CrossRef]
14. Kong, F.; Li, G.; Wang, J.; Shi, Y.; Zhou, R. Promoting effect of acid sites in hierarchical porous Pt/ZSM-5 catalysts for low-temperature removal of VOCs. *Appl. Surf. Sci.* **2022**, *606*, 154888. [CrossRef]
15. El-Bahy, Z.M.; Alotaibi, M.T.; El-Bahy, S.M. CO oxidation and 4-nitrophenol reduction over ceria-promoted platinum nanoparticles impregnated with ZSM-5 zeolite. *J. Rare Earths* **2022**, *40*, 1247–1254. [CrossRef]
16. Wang, J.; Shi, Y.; Kong, F.; Zhou, R. Low-temperature VOCs oxidation performance of Pt/zeolites catalysts with hierarchical pore structure. *J. Env. Environ. Sci.* **2023**, *124*, 505–512. [CrossRef]
17. Tsou, J.; Magnoux, P.; Guisnet, M.; Órfão, J.M.; Figueiredo, J.L. Catalytic oxidation of volatile organic compounds: Oxidation of methyl-isobutyl-ketone over Pt/zeolite catalysts. *Appl. Catal. B Env. Environ.* **2005**, *57*, 117–123. [CrossRef]
18. Chen, C.; Chen, F.; Zhang, L.; Pan, S.; Bian, C.; Zheng, X.; Meng, X.; Xiao, F.S. Importance of platinum particle size for complete oxidation of toluene over Pt/ZSM-5 catalysts. *Chem. Commun.* **2015**, *51*, 5936–5938. [CrossRef]
19. López-Fonseca, R.; Gutiérrez-Ortiz, J.I.; Gutiérrez-Ortiz, M.A.; González-Velasco, J.R. Catalytic oxidation of aliphatic chlorinated volatile organic compounds over Pt/H-BETA zeolite catalyst under dry and humid conditions. *Catal. Today* **2005**, *107–108*, 200–207. [CrossRef]
20. Kummer, J.T. Oxidation of CO and C_2H_4 by Base Metal Catalysts Prepared on Honeycomb Supports. In *Advances in Chemistry*; Evoy, M., Ed.; Series 143; American Chemical Society: Washington, DC, USA, 1975; pp. 178–192. [CrossRef]
21. Walker, S.; Straguzzi, G.I.; Manogue, W.H.; Schuit, G.C.A. Carbon monoxide and propene oxidation by iron oxides for auto-emission control. *J. Catal.* **1988**, *110*, 298–309. [CrossRef]
22. Li, P.; Miser, D.E.; Rabiei, S.; Yadav, R.T.; Hajaligol, M.R. The removal of carbon monoxide by iron oxide nanoparticles. *Appl. Catal. B Environ.* **2003**, *43*, 151–162. [CrossRef]
23. Szegedi, A.; Hegedus, M.; Margitfalvi, J.L.; Kiricsi, I. Low temperature CO oxidation over iron-containing MCM-41 catalysts. *Chem. Commun.* **2005**, *11*, 1441–1443. [CrossRef] [PubMed]
24. Rangus, M.; Mazaj, M.; Dražić, G.; Popova, M.; Tušar, N.N. Active Iron Sites of Disordered Mesoporous Silica Catalyst FeKIL-2 in the Oxidation of Volatile Organic Compounds (VOC). *Materials* **2014**, *7*, 4243–4257. [CrossRef]
25. Jianga, X.C.; Yu, A.B. Synthesis of Pd/α-Fe_2O_3 nanocomposites for catalytic CO oxidation. *J. Mater. Process Technol.* **2009**, *209*, 4558–4562. [CrossRef]
26. Shao, J.; Zhai, Y.; Zhang, L.; Xiang, L.; Lin, F. Low-Temperature Catalytic Ozonation of Multitype VOCs over Zeolite-Supported Catalysts. *Int. J. Environ. Res. Public Health* **2022**, *19*, 14515. [CrossRef] [PubMed]
27. Yang, L.; Liu, Q.; Han, R.; Fu, K.; Su, Y.; Zheng, Y.; Wu, X.; Song, C.; Ji, N.; Lu, X.; et al. Confinement and synergy effect of bimetallic Pt-Mn nanoparticles encapsulated in ZSM-5 zeolite with superior performance for acetone catalytic oxidation. *Appl. Catal. B Environ.* **2022**, *309*, 121224. [CrossRef]

28. Li, S.; Liu, G.; Lian, H.; Jia, M.; Zhao, G.; Jiang, D.; Zhang, W. Low-temperature CO oxidation over supported Pt catalysts prepared by colloid-deposition method. *Catal. Commun.* **2008**, *9*, 1045–1049. [CrossRef]
29. Li, J.; Xiao, G.; Guo, Z.; Lin, B.; Hu, Y.; Fu, M.; Ye, D. ZSM-5-supported V-Cu bimetallic oxide catalyst for remarkable catalytic oxidation of toluene in coal-fired flue gas. *Chem. Eng. J.* **2021**, *419*, 129675. [CrossRef]
30. Jodaei, A.; Salari, D.; Niaei, A.; Khatamian, M.; Çaylak, N. Preparation of Ag–M (M: Fe, Co and Mn)–ZSM-5 bimetal catalysts with high performance for catalytic oxidation of ethyl acetate. *Environ. Technol.* **2011**, *32*, 395–406. [CrossRef]
31. Shabani, J.M.; Ameh, A.E.; Oyekola, O.; Babajide, O.O.; Petric, L. Fusion-Assisted Hydrothermal Synthesis and Post-Synthesis Modification of Mesoporous Hydroxy Sodalite Zeolite Prepared from Waste Coal Fly Ash for Biodiesel Production. *Catalysts* **2022**, *12*, 1652. [CrossRef]
32. Hui, K.S.; Chao, C.Y.H. Conversion of coal fly ash into zeolite 4A and its applications in waste eater treatment and greenhouse gas reduction. In Proceedings of the IMECE2007, Seattle, WA, USA, 11–15 November 2007. [CrossRef]
33. Boycheva, S.; Zgureva, D.; Vaclavıkova, M.; Kalvachev, Y.; Lazarova, H.; Popova, M. Studies on non-modified and copper-modified coal ash zeolites as heterogeneous catalysts forVOCs oxidation. *J. Hazard. Mater.* **2019**, *361*, 374–382. [CrossRef] [PubMed]
34. Popova, M.; Boycheva, S.; Lazarova, H.; Zgureva, D.; Lázár, K.; Szegedi, Á. VOC oxidation and CO_2 adsorption on dual adsorption/catalytic system based on fly ash zeolites. *Catal. Today* **2020**, *357*, 518–525. [CrossRef]
35. Todorova, S.; Barbov, B.; Todorova, T.; Kolev, H.; Ivanova, I.; Shopska, M.; Kalvachev, Y. CO oxidation over Pt-modified fly ash zeolite X. *React. Kinet. Mech. Cat.* **2020**, *129*, 773–786. [CrossRef]
36. Treacy, M.M.J.; Higgins, J.B. (Eds.) *Collection of Simulated XRD Powder Patterns for Zeolites, Structure Commision of the International Zeolite Association*, 4th ed.; Elsevier: Amsterdam, The Netherlands, 2001.
37. Rayalu, S.; Udhoji, J.; Meshram, S.; Naidu, R.; Devotta, S. Estimation of crystallinity in fly ash-based zeolite-A using XRD and IR spectroscopy. *Curr. Sci.* **2005**, *89*, 2147–2151. Available online: https://www.jstor.org/stable/24111077 (accessed on 19 March 2023).
38. Majchrzak-Kuceba, I. A simple thermogravimetric method for the evaluation of the degree of fly ash conversion into zeolite material. *J. Porous Mater.* **2013**, *20*, 407–415. [CrossRef]
39. Mos, Y.M.; Vermeulen, A.C.; Buisman, C.J.N.; Weijm, J. X-Ray Diffraction of Iron Containing Samples: The Importance of a Suitable Configuration. *Geomicrobiol. J.* **2018**, *35*, 511–517. [CrossRef]
40. Huang, H.; Ji, Y.; Qiao, Z.; Zhao, C.; He, J.; Zhang, H. Preparation, Characterization, and Application of Magnetic Fe-SBA-15 Mesoporous Silica Molecular Sieves. *J. Anal. Methods Chem.* **2010**, *2010*, 323509. [CrossRef]
41. Ma, I.-K.; Rigolet, S.; Michelin, L.; Paillaud, J.-L.; Mintova, S.; Khoerunnisa, F.; Daou, T.; Ng, E. Facile and fast determination of Si/Al ratio of zeolites using FTIR spectroscope technique. *Microporous Mesoporous Mater.* **2021**, *311*, 110683. [CrossRef]
42. Ono, L.K.; Yuan, B.; Heinrich, H.; Cuenya, B.R. Formation and Thermal Stability of Platinum Oxides on Size-Selected Platinum Nanoparticles: Support Effects. *J. Phys. Chem. C* **2010**, *114*, 22119–22133. [CrossRef]
43. Moulder, F.; Sticke, W.F.; Sobol, P.E.; Bombel, K.D. *Handbook of X-ray Photoelectron Spectroscopy*, 2nd ed.; Perkin-Elmer Corporation, Physical Electron Division: Eden Prairie, MN, USA, 1992.
44. Grunthaner, P.J.; Grunthaner, F.J.; Madhukar, A. Chemical bonding and charge redistribution: Valence band and core level correlations for the Ni/Si, Pd/Si, and Pt/Si systems. *J. Vac. Sci. Technol.* **1982**, *20*, 680–683. [CrossRef]
45. Oku, M.; Hirokawa, K. X-ray photoelectron spectroscopy of Co_3O_4, Fe_3O_4, Mn_3O_4, and related compounds. *J. Electron. Spectrosc. Relat. Phenom.* **1976**, *8*, 475–481. [CrossRef]
46. Nefedov, V.I.; Salyn, Y.V.; Leonhardt, G.; Scheibe, R. A comparison of different spectrometers and charge corrections used in X-ray photoelectron spectroscopy. *J. Electron. Spectrosc. Relat. Phenom.* **1977**, *10*, 121–124. [CrossRef]
47. Allen, G.C.; Curtis, M.T.; Hooper, A.J.; Tucker, P.M. X-Ray photoelectron spectroscopy of iron–oxygen systems. *J. Chem. Soc. Dalton Trans.* **1974**, *14*, 1525–1530. [CrossRef]
48. McIntyre, N.S.; Zetaruk, D.G. X-ray photoelectron spectroscopic studies of iron oxides. *Anal. Chem.* **1977**, *49*, 1521–1529. [CrossRef]
49. Pineau, A.; Kanari, N.; Gaballah, I. Kinetics of reduction of iron oxides by H_2: Part I: Low temperature reduction of hematite. *Thermochim. Acta* **2006**, *447*, 89–100. [CrossRef]
50. Hea, C.; Li, J.; Li, P.; Chenga, J.; Haoa, Z.; Xu, Z.-P. Comprehensive investigation of Pd/ZSM-5/MCM-48 composite catalysts with enhanced activity and stability for benzene oxidation. *Appl. Catal. B Environ.* **2010**, *96*, 466–475. [CrossRef]
51. Li, J.; Feng, Y.; Mo, S.; Liu, H.; Chen, Y.; Yang, J. Nanodendritic Platinum Supported on γ-Alumina for Complete Benzene Oxidation. *Part. Part. Syst. Charact.* **2016**, *33*, 620–627. [CrossRef]
52. Tabakova, T.; Ilieva, L.; Petrova, P.; Venezia, A.M.; Avdeev, G.; Zanella, R.; Karakirova, Y. Complete benzene oxidation over mono and bimetallic Au–Pd catalysts supported on Fe-modified ceria. *Chem. Eng. J.* **2015**, *260*, 133–141. [CrossRef]
53. Ilieva, L.; Petrova, P.; Venezia, A.M.; Anghel, E.; State, R.; Avdeev, G.; Tabakova, T. Mechanochemically prepared Co_3O_4-CeO_2 catalysts for complete benzene oxidation. *Catalysts* **2021**, *11*, 1316. [CrossRef]
54. Tomatis, M.; Xu, H.; Wei, C.; Bishop, M.; He, J.; Wang, C.; Zhao, M.; Xiao, H.; Yu, H.; Behera, S.N.; et al. A Comparative Study of Mn/Co Binary Metal Catalysts Supported on Two Commercial Diatomaceous Earths for Oxidation of Benzene. *Catalysts* **2018**, *8*, 111. [CrossRef]
55. Tabakova, T.; Ilieva, L.; Petrova, P.; Venezia, A.M.; Karakirova, Y.; Liotta, L.; Avdeev, G. Complete benzene oxidation over mono and bimetallic Pd-Au catalysts on Alumina supported Y-dopped ceria. *Appl. Sci.* **2020**, *10*, 1088. [CrossRef]

56. Scofield, J.H. Hartree-Slater subshell photoionization cross-sections at 1254 and 1487 eV. *J. Electron. Spectrosc. Relat. Phenom.* **1976**, *8*, 129–137. [CrossRef]
57. Monti, D.A.M.; Baiker, A. Temperature-programmed reduction. Parametric sensitivity and estimation of kinetic parameters. *J. Catal.* **1983**, *83*, 323–335. [CrossRef]